ADVANCES IN ATMOSPHERIC SCIENCES, VOL. 30, NO. 2, 2013, 448–460

Application of Multi-Scale Tracking Radar Echoes Scheme in Quantitative Precipitation Nowcasting

WANG Gaili*[1] (王改利), WONG Waikin[2] (黄伟健),
LIU Liping[1] (刘黎平), and WANG Hongyan[1] (王红艳)

[1]*State Key Laboratory of Severe Weather, Chinese Academy of Meteorological Science, Beijing* 100081

[2]*Hong Kong Observatory, Hong Kong* 999077

(Received 29 February 2012; revised 27 June 2012)

ABSTRACT

A new radar echo tracking algorithm known as multi-scale tracking radar echoes by cross-correlation (MTREC) was developed in this study to analyze movements of radar echoes at different spatial scales. Movement of radar echoes, particularly associated with convective storms, exhibits different characteristics at various spatial scales as a result of complex interactions among meteorological systems leading to the formation of convective storms. For the null echo region, the usual correlation technique produces zero or a very small magnitude of motion vectors. To mitigate these constraints, MTREC uses the tracking radar echoes by correlation (TREC) technique with a large "box" to determine the systematic movement driven by steering wind, and MTREC applies the TREC technique with a small "box" to estimate small-scale internal motion vectors. Eventually, the MTREC vectors are obtained by synthesizing the systematic motion and the small-scale internal motion. Performance of the MTREC technique was compared with TREC technique using case studies: the Khanun typhoon on 11 September 2005 observed by Wenzhou radar and a squall-line system on 23 June 2011 detected by Beijing radar. The results demonstrate that more spatially smoothed and continuous vector fields can be generated by the MTREC technique, which leads to improvements in tracking the entire radar reflectivity pattern. The new multi-scale tracking scheme was applied to study its impact on the performance of quantitative precipitation nowcasting. The location and intensity of heavy precipitation at a 1-h lead time was more consistent with quantitative precipitation estimates using radar and rain gauges.

Key words: multi-scale tracking, extrapolation, nowcasting

Citation: Wang, G. L., W. Wong, L. P. Liu, and H. Y. Wang, 2013: Application of multi-scale tracking radar echoes scheme in quantitative precipitation nowcasting. *Adv. Atmos. Sci.*, **30**(2), 448–460, doi: 10.1007/s00376-012-2026-7.

1. Introduction

Heavy rain is one of the most severe weather events in China, causing floods and other geological and hydrological disasters. Many severe and widespread floods have occurred in recent decades, for example, the summer floods in southern China in 1991 and 1998. To enhance the monitoring of severe convective systems, and to mitigate disasters resulting from heavy rain and flooding, a national network of Doppler radars has recently been implemented, operated by the China Meteorological Administration (CMA). This modernized radar network has become the primary and indispensable observation platform for severe weather warning. Some advantages of this network are nationwide coverage, Doppler capabilities, and high spatial and temporal resolution. These advantages advance the detection of weather events, support forecasting and warning services, and reduce natural disasters. A number of techniques for the short-term forecasting of severe weather have been developed in the last several decades for extrapolating observed radar patterns into the following 1–3 h. These nowcasting techniques are classified into three major groups Lakshmanan et al., 2003. The first group has the ability to identify 3D storm structures and to track and forecast

*Corresponding author: WANG Gaili, wgl3111@cams.cma.gov.cn

storm-related characteristic parameters such as areas, mass centroids, and maximum reflectivity (Dixon and Wiener, 1993; Johnson et al., 1998). Another nowcasting technique uses an artificial neural network (ANN) algorithm as a statistical learning method to predict future locations of precipitation (French et al., 1992). Limitations of the technique include the requirement of training the ANN in real time, and the fact that a trained neural network cannot produce forecasts that have not been tracked during a training phase (Lakshmanan et al., 2003). The third technique considers radar echo movement between two consecutive radar patterns. This common robust technique to estimate echo movement is called tracking radar echoes by correlation (TREC; Rinehart and Garvey, 1978; Tuttle and Gall, 1999).

Several variants or modifications of this correlation-based technique were investigated for estimation of radar echo motion at different spatial scales. For example, pre-processing or filtering of a reflectivity field can be used to track echoes only at larger scales (Wolfson et al., 1999; Lakshmanan et al., 2000). Both centroid trackers and pattern-matching methods are considered most reliable for convective quantitative precipitation nowcasting (QPN). However, for widespread and stratiform precipitation events, the pattern-matching methods are considered superior to centroid tracking techniques, for which individual convective cells cannot be easily distinguished (Pierce et al., 2004).

The cross-correlation method was first used to determine the entire radar pattern motion in the 1960s (Kessler and Russo, 1963). The technique was then modified to obtain the internal motion of small-scale radar echoes (Rinehart and Garvey, 1978; Tuttle and Foote, 1990). To reduce the influence of "noisy" vectors, often caused by ground clutter, shielding (Tuttle and Foote, 1990), and small-scale changes within the radar patterns (Rinehart, 1981), COTREC (continuity of TREC vectors) was presented based on constraints used in a variational technique (Li et al., 1995). Although echoes extrapolated by the new vectors were much smoother and more continuous, the COTREC technique did not completely eliminate the zero vectors, small vectors, and the vectors with directions opposite their adjacent vectors (Li et al., 1995). Another technique, difference image-based tracking radar echo by correlations (DITREC) was proposed to eliminate the disorder vectors of TREC vectors caused by the rapid changes of echoes. However, DITREC results in some pixels at less than threshold values to be ignored (Zhang et al., 2006). To extend the extrapolation algorithm for QPN up to 3 h ahead, a blending approach has also been proposed that combines TREC vectors with model-predicted winds (Liang et al., 2010).

Moving directions of echoes at different scales are not always consistent (Houze et al., 1993). Storm motion is also considered as a combination of steering-level winds and internal motion (Germann et al., 2006). Sometimes the systemic motion of a precipitation system is ignored in the TREC method due to grid division of the radar reflectivity field into a number of small "boxes". At the same time, zero vectors are estimated over areas with a null echo, initial echo development, and widespread weak echoes. Growth and decay of echoes often produce discontinuous forecast fields. Therefore, a multi-scale tracking radar echoes by correlation (MTREC) was proposed in this study. MTREC first uses the TREC technique with a large "box" to determine the systematic movement of the echoes driven by steering-level wind between two consecutive images at t_0 and t_1. In this technique, a semi-Lagrangian advection calculation is used extrapolate the echo field from time t_0 to the time t_1. Then the TREC method with small "box" is applied to compute small-scale internal motion vectors of radar patterns. The final MTREC motion vectors are obtained by synthesizing the systemic motion and the internal motion. In this way, both the large-scale motion of the whole precipitation system and small-scale movement of the embedded storm cells can be taken into account in MTREC. Generation of zero vectors can then be avoided because the motion field over the null echo region is specified by the large-scale motion for the primary radar reflectivity pattern.

2. Data description

The radar data were obtained from the operational weather radar network of the CMA. The parameters of the radar, such as data formats and volume scan pattern (VCPs), were the standard precipitation observation modes of VCP21. The rain-gauge data used in radar quantitative precipitation estimate (QPE) scheme were obtained from the operational rain-gauge stations of the CMA, with spatial separations of ∼10 km.

To compare the MTREC vectors with radar Doppler measurements, single radar data were used in this study to track and nowcast precipitation fields. With respect to QPN, the movement of near-surface precipitation was expected. In this study, the MTREC and TREC vectors were determined using radar constant altitude plan position indicator (CAPPI) at the height of 3 km, which provided appropriate radar observation range and were not affected by the bright band layer (Steiner et al., 1995). The CAPPIs were provided by the Doppler Weather Radar 3-D Digital

Mosaic System, which was developed by the State Key Laboratory of Severe Weather of the Chinese Academy of Meteorological Science (Wang et al., 2009). Quality control was first performed for single radar reflectivity data to remove electronic interference, ground clutter, and anomalous propagations. The 3D Cartesian-gridded reflectivity data were then interpolated from the spherical coordinate system. The data had a high horizontal resolution of 0.01° (lat)×0.01° (lon) (∼1 km ×1 km), and high temporal resolution of 6 min (Xiao et al., 2008; Wang et al., 2009).

3. Description of MTREC scheme

The major steps of MTREC are outlined as follows:

(1) Determine the systematic motions of overall echoes;

(2) Advect the echo field from time t_0 to t_1;

(3) Using the extrapolated radar echo field from step (2) and the one at time t_1, compute internal motion vectors;

(4) Synthesize the motion fields from steps (2) and (3) above and apply a smoothing procedure to generate the final gridded motion vectors.

Details of the computation steps are given in the following sections.

3.1 *Determine the systematic motions of overall echoes*

Taking into account the systematic movement of heavy rain, the systematic motion of overall echoes is determined using TREC technique with large "box" because a large "box" can determine the general mean motion on a broad echoes scale (Tuttle and Foote, 1990). The reflectivity pattern is divided into a number of equal "boxes". The motion vector over a "box" is assumed uniform and is determined by calculating the maximum correlation coefficient between two consecutive reflectivity patterns. The correlation is calculated in the search radius using

$$R_{(p,q)} = \frac{\sum_{i=1}\sum_{j=1}[m(i+p,j+q,t_1)-\overline{m}(t_1)][m(i,j,t_0)-\overline{m}(t_0)]}{\left\{\sum_{i=1}\sum_{j=1}[m(i+p,j+q,t_1)-\overline{m}(t_1)]^2\sum_{i=1}\sum_{j=1}[m(i,j,t_0)-\overline{m}(t_0)]^2\right\}^{\frac{1}{2}}}, \quad (1)$$

where $m(i, j, t_0)$ and $m(i, j, t_1)$ represent reflectivity observations at time t_0 and t_1, respectively; p and q indicate components of a motion vector; i, j, $i + p$, and $j + q$ are grid positions; $\overline{m}$ denotes the average reflectivity of the "box". The displacement vector corresponding with the maximum correlation coefficient is regarded as the motion over the "box". A search radius $R = v_{\max} \times \Delta t$ is used to limit the greatest displacement, where $v_{\max}$ is the maximum storm velocity.

The cross-correlation method was originally used to determine the overall movement of radar pattern. Theoretically, the single motion vector can denote the systematic motion of radar pattern. However, for those rotating precipitation systems like typhoons, the single motion vector does not represent systematic rotation. To overcome the drawback, in this study, we assumed the systematic movement to include several motion vectors at four orientations of radar pattern. Thus the TREC technique with large "boxes" was used to produce the systematic movement. To obtain stable systematic movement, three schemes were tested: "box" sizes of 1.0° (∼100 km), 1.5° (∼150 km) and 2.0° (∼200 km), and the "box" size of 1.5° (∼150 km) was selected for good data consistency, and small standard deviation (SD).

3.2 *Extrapolate the echo field from time t_0 to t_1*

The semi-Lagrangian method is one of the major numerical schemes used to calculate fluid motion. Characterized by permission rotation, conservation of mass, good computational stability and accuracy of calculation, the semi-Lagrangian method has been widely applied to numerical weather prediction and climate models. The forecasts from a Lagrangian radar echo extrapolation scheme (MAPLE) clearly outperformed Eulerian persistence forecasts for all the lead times and showed better accuracy compared to high-resolution numerical weather prediction model (COSMO2) up to lead time of 3 h on average (Pradeep et al., 2012). In this study, a remapped particle-mesh semi-Lagrangian (RPMSL) advection scheme (Reich, 2007) was used to extrapolate echo or precipitation fields from time t_0 to time t_1. The explicit RPMSL advection scheme used bilinear and bicubic B-splines as basic approximation functions. The detail computation of gridded reflectivity field at time t_1 based on given gridded reflectivity field and velocity field at time t_0 were adopted from Reich (2007).

3.3 *Compute internal motion vectors*

The explicit RPM SL scheme was used to extrapolate the radar pattern from t_0 to t_1. The internal motion vectors were obtained based on the radar extrapolation pattern and the radar observation pattern at t_1 using the TREC technique with a small "box". This step was similar to those described in section 3.1, except for the size of "box".

In this step, a box size of 0.2° (∼20 km) and grid spacing of 0.1° (∼10 km) were selected to determine the internal motion, considering stratiform and convective precipitation.

3.4 *Computation of MTREC vectors*

The MTREC vectors were obtained by combining or synthesizing the internal motion vectors and the systematic motion vectors. To reduce the influence of "noisy" vectors as results of ground clutter, shielding, and/or instability in obtaining vector fields using maximum correlation, consistency of the data was first verified for each motion vector. Then the two components of the MTREC vector fields were objectively analyzed using the Cressman-weighting function (Li et al., 2000; Wang et al., 2007).

4. Performance

Two case studies were selected to compare the MTREC vectors with TREC vectors and radar Doppler measurement: Khanun typhoon on 11 September 2005 observed by Wenzhou CINRAD/SA radar and a squall line system on 23 June 2011 detected by Beijing CINRAD/SA radar. Because of the changes in echoes resulting in chaotic vectors in TREC vectors, Rinehart (1981) proposed that the time interval is preferably less than 5 min in the application of TREC technology. In this study, the time interval of the two continuous radar images was six min, which corresponds to the time resolution of the Doppler weather radar precipitation patters set by the CMA. The maximum speed constraint of $v_{\max}$=100 km h^{-1} was used in this study (Han et al., 2009). Those vectors with correlation coefficients <0.25 were discarded (Tuttle and Foote, 1990).

The strong Khanun typhoon formed over the northwest of the Pacific Ocean on 7 September 2005, and it moved northwest and made landfall at 0651 UTC 11 September in Taizhou, Zhejiang. Two consecutive radar patterns at 0300 UTC (Fig. 1a) and 0306 UTC (Fig. 1b) 11 September 2005 were selected for the comparison of MTREC vectors and TREC vectors. Figures. 1c, e, and f show three systemic motions, obtained using the TREC technique with three "box" sizes: 1.0° (∼100 km), 1.5° (∼150 km) and 2.0° (∼200 km), respectively. The corresponding MTREC vector fields are given in Figs. 1d, f, and g. The three sizes of large "box" schemes for retrieving systemic motion and corresponding MTREC vector fields are all consistent, rotary, and without zero vectors. Furthermore, the systemic motion obtained using the TREC technique with a "box" size of 1.5° (∼150 km; Fig. 1e) and the corresponding MTREC vector field (Fig. 1f) are more consistent and have smaller SD than the other two schemes. Though the TREC vector field (Fig. 1i) also detected the rotational motion of the typhoon, zero vectors existed over null echoes and small chaotic vectors were present at the edge of echoes, resulting in less consistency and higher SD compared with the MTREC vector field.

Because there was little vertical wind shear in the cloud layer of the hurricane/typhoon, the retrieval wind fields using the TREC method were in agreement with Doppler radar radial velocities (Tuttle and Gall, 1999). In case of the Khanun typhoon, we also computed the radial component of each MTREC vector and compared it to the radar Doppler radial velocity smoothed with a 20-km (∼0.2°) filter window. The quantitative statistics are given in Fig. 1j, showing a scattergram and the correlation coefficient (CC) and the RMSE. A CC of 0.99 and an RMSE of 4.93 m s^{-1} indicate good agreement and little difference between MTREC and Doppler observations.

The squall line system on 23 June 2011 produced the largest amount of precipitation during one event in the last decade in Beijing. The movement of the squall line is illustrated in Figs. 2a–d, which show the patterns of radar reflectivity in time intervals of 18 and 12 min, respectively. The whole squall line was situated southwest to northeast and moved southeasterly. However, the movements of echoes varied considerably over the whole squall-line system. The echoes at the middle of the squall line moved mainly easterly, while the echoes at the edge of the squall line moved southeasterly.

The two continuous radar patterns at 3 km height, measured using CAPPI at 1024 and 1030 UTC 23 June 2011 were used to obtain TREC vectors and MTREC vectors. For this squall line event, there was little difference among three schemes of systemic motion using the TREC technique with "box" sizes of 1.0° (∼100 km), 1.5° (∼150 km), and 2.0° (∼200 km), respectively. The "box" size of 1.5°(∼150 km) was also selected to determine systemic movement in this event. TREC vectors (Fig. 2e) and MTREC vectors (Fig. 2f) were processed using the same consistency check and objective analysis. Although TREC vectors were basically in agreement with the MTREC vectors across most of the area, a significant difference could easily

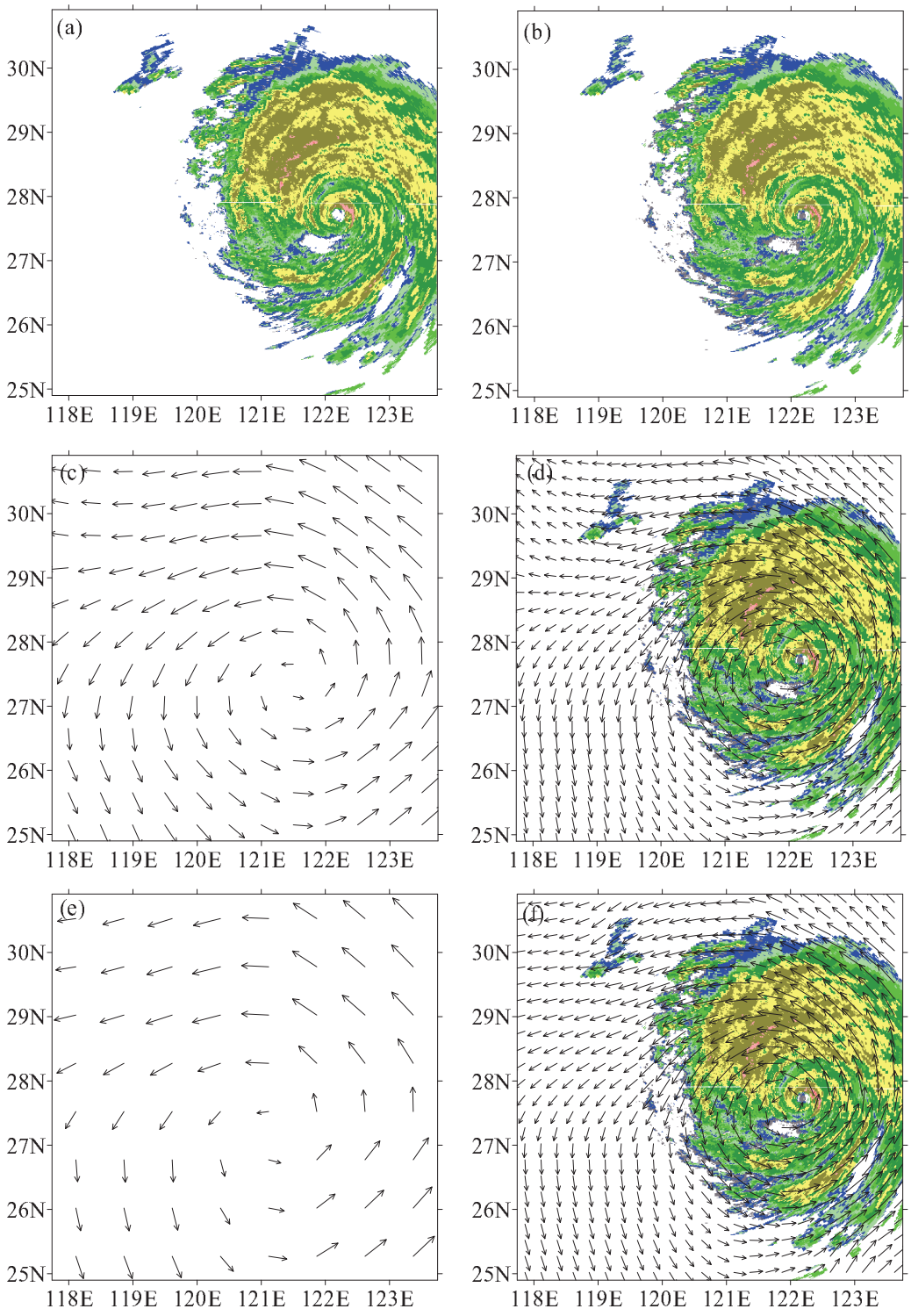

Fig. 1. Assessment of MTREC vector fields for Khanun typhoon retrieved from two consecutive radar patterns at (a) 0300 and (b) 0306 UTC 11 September 2005 observed by Wenzhou radar. The systemic motions are derived using TREC technique with three "box" sizes of (c) 1.0° (∼100 km), (e) 1.5° (∼150 km), and (g) 2.0° (∼200 km), respectively and (d, f, and h) corresponding MTREC vectors with spatial resolution of 0.1° (∼10 km). Comparison MTREC vectors with (i) TREC vectors and (j) radar Doppler radial velocities.

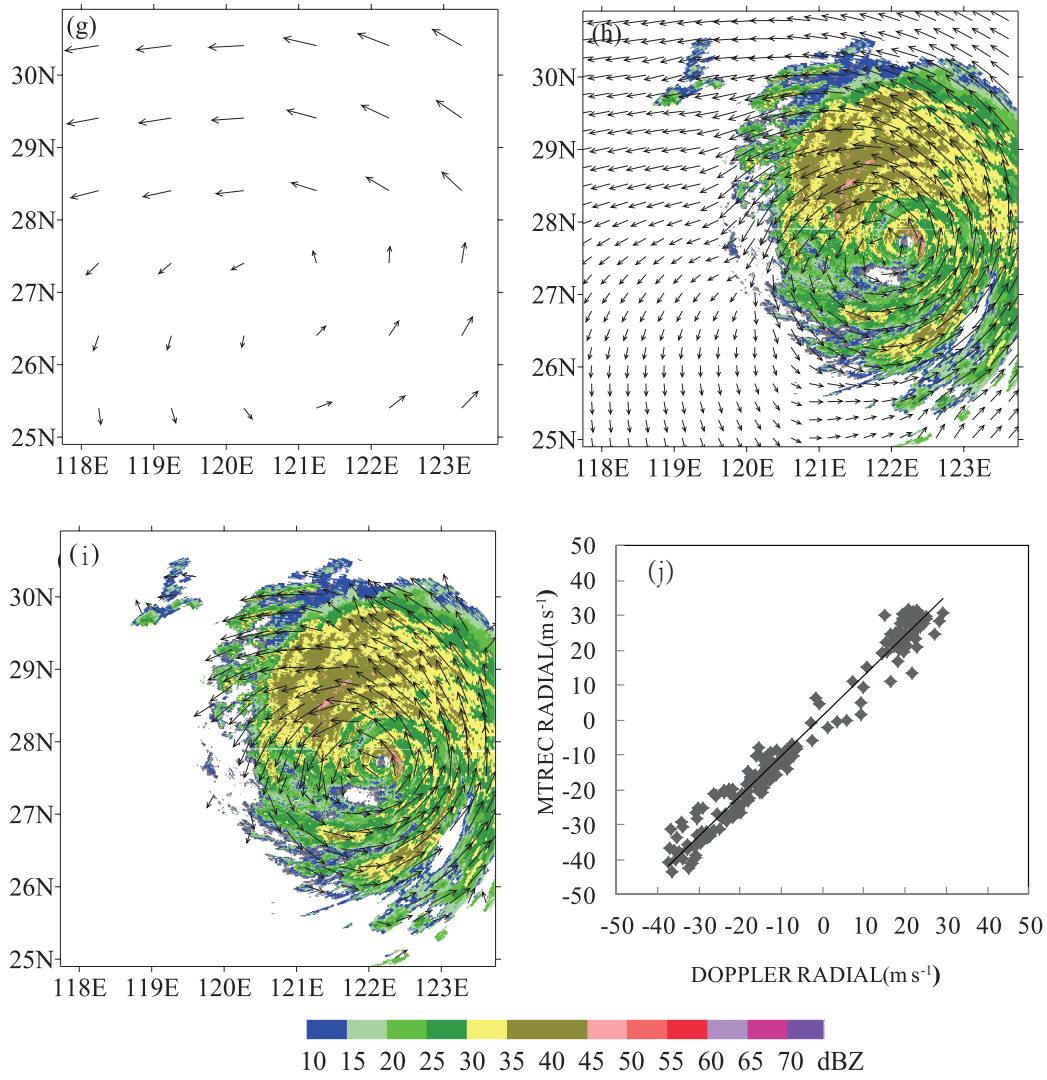

Fig. 1. (Continue).

be seen in the area near 40°N, 118°E. The retrieved motion vectors in that area using the TREC technique moved northeast, while those using the MTREC technique moved southeast. Based on the Figs. 2a–d, the echoes in that area moved southeast. In addition, in Fig. 2e, because less effective radar data were included in arrays at the edge of echoes, erratic motion vectors occurred that could not be eliminated, even after objective analysis. In Fig. 2f, MTREC vectors are smoother and did not show any erratic motion at the edge regions. The motion of the overall squall line in the MTREC moved southeast, consistent with the motion of the squall line (Figs. 2a–d). The zero vectors over the null echo region were replaced by motion vectors of the whole image, which could make more continuous extrapolation of echoes.

When tracking the motion of convective precipitation, due to the effects of strongly vertical wind shear, the advection mainly determines precipitation motion, which may disagree with the Doppler measurements (Tuttle and Foote, 1990; Tuttle and Gall, 1999; Zhang et al., 2006). Therefore, for this squall event, we analyzed the Doppler radial velocities instead of comparing the radial components of MTREC vectors to them.

The wind shear is also strongly vertical in the squall line case. The Doppler radial velocities of 1.4° elevation at 1030 UTC 23 June 2011 are shown in Fig. 2g. The wind shear is strongly vertical at the altitude of ∼3 km, and the direction of high level steering flow was west–southwest. Studies have shown that the storms in zonal thunderstorm systems move along somewhat to the right of the average steering flow (Li et al., 2004; Yao et al., 2005). Therefore,

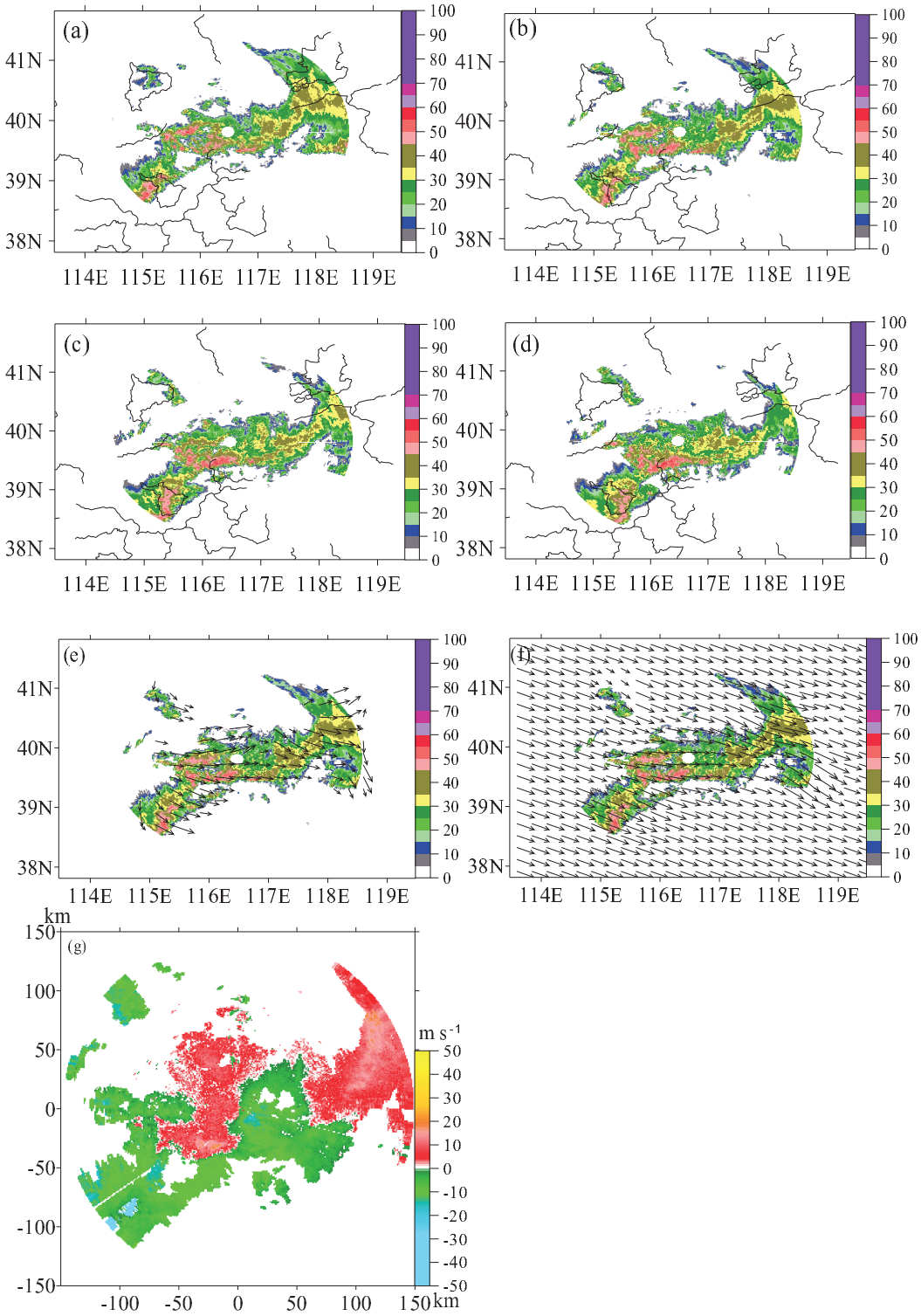

Fig. 2. The patterns of 3-km CAPPI reflectivity at (a) 1012, (b) 1030, (c) 1048, and (d) 1100 UTC for the squall line observed by Beijing radar on 23 June 2011. (e) TREC vectors and (f) MTREC vectors based on pairs of CAPPIs that were obtained at 1024 and 1030 UTC, and (g) the radar Doppler measurement of 1.4° at 1030 UTC on 23 June 2011.

the squall line in this study moved east–southeast, in agreement with the retrieval MTREC vectors. For the most widespread precipitation, the MTREC motion fields were similar to those of the TREC. However, MTREC motion fields were smoother, more continuous, and without zero vectors.

5. Quantitative precipitation nowcasting scheme

The explicit RPMSL scheme described in section 3.2 was used to extrapolate radar patterns at a lead time because of its permission of rotation and mass conservation. The forecast of the Khanun typhoon based on the explicit RPMSL scheme is given in Fig. 3, which qualitatively shows that the explicit RPMSL scheme is able to conserve the rotary shape of the typhoon system.

The integration step of a semi-Lagrangian advection scheme was set to 15 min, and the forecast fields were output in 15-min intervals. The forecast at lead time was obtained by averaging the outputs in 1 h.

Conventionally, QPN scheme is the reflectivity field extrapolated based on retrieved motion fields, and then reflectivity–rainfall rate (Z–R) relationship is used to convert echo intensity to rainfall. However, radar QPE is affected by radar parameters, inappropriate Z–R relationship, rainstorm attenuations, bright bands, and ground clutter contamination (Wilson and Brandes, 1979; Zawadzki, 1984; Zhang et al., 2001). The inaccurate Z–R relation is one of the main contributors of radar rainfall underestimation based on reflectivity observations (Baeck and Smith, 1998). To reduce forecast precipitation errors, instead of radar reflectivity pattern, 1-h QPE combining radar and rain-gauges was extrapolated using the explicit RPMSL advection scheme.

In this study, a two-step correction technique of radar QPE was used to estimate quantitative precipitation (Wang et al., 2012). Real-time adjustment to the Z–R relationship scheme was first used to remove systematic bias on the time-domain, and the gauge-corrected radar-based estimates scheme with inverse distance weighting interpolation were then used to eliminate non-uniform errors in space. In other studies, results have shown that this two-step correction technique have been shown to improve QPE by reducing both the systematic average bias and the spatial error (Wang et al., 2012).

Due to raindrops of different sizes falling at different rates and the delay of data being uploaded, radar reflectivity was averaged for each pixel every 30 min and then was matched to the rain-gauge observations. An optimized Z–R relationship was fitted using radar–rain–gauge (R–G) pairs every 30 min.

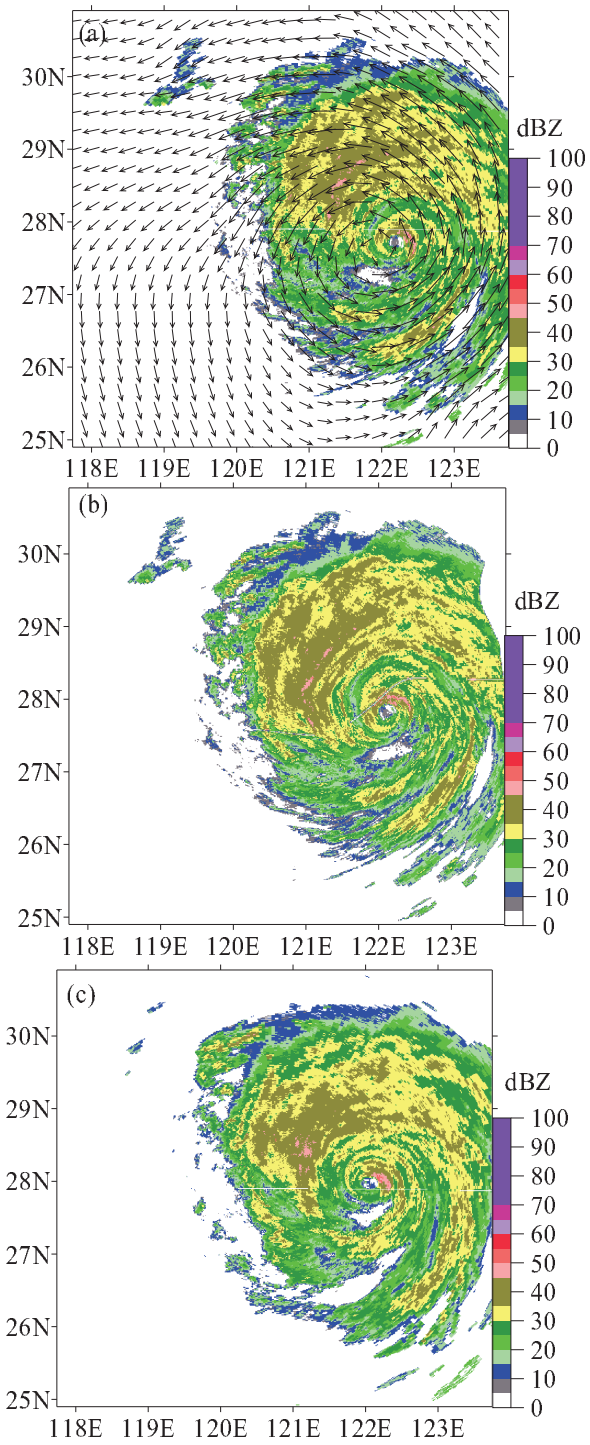

Fig. 3. (a) MTREC vector field retrieved from consecutive reflectivity CAPPIs at 0300 and 0306 UTC 11 September 2005 and (b) forecast reflectivity field of typhoon Khanun obtained by semi-Lagrangian advection (b) at lead time of 1 h, and (c) simultaneous observation.

The procedure of the local bias correction scheme was used to calculate an additive radar rainfall error at each rain-gauge location, and these errors were then interpolated over all of the radar reflectivity patterns at 3-km CAPPI using the following equation:

$$e = \frac{\sum_{i=1}^{n} e_i w_i}{\sum_{i=1}^{n} w_i} , \tag{2}$$

where e is the estimated radar error at the pixel being interpolated, w_i is the weight assigned to the ith rain gauge, and n represents the total number of matching R–G pairs. Each pixel of the QPE field is corrected by e. The inverse distance weighting (IDW) was used to calculate correction factors at each pixel of radar-based QPE fields in this study. The weights were calculated using the following equation (Ware, 2005):

$$w_i = \begin{cases} \dfrac{1}{d_i^m} & d_i \leqslant R \\ 0 & d_i > R \end{cases} , \tag{3}$$

where d_i denotes the distance between the radar grid point and the ith rain gauge, R is the radius of influence of the radar grid point, and m is an exponent. There are different weights for each radar pixel on each rain gauge. Two parameters are the specified radius R and the exponent m, in the inverse distance weighting. Cross-validation was used to calculate the optimum parameter values.

6. Case studies

To assess the MTREC schemes and QPN, we chose to analyze the following case studies: on 11 September 2005 the Khanun typhoon observed by Wenzhou CINRAD/SA radar and a squall line system on 23 June 2011 detected by Beijing CINRAD/SA radar. To evaluate the forecast skill, both the forecast rainfall fields and the observation rainfall fields obtained using two-step correction technique were mapped onto a $0.01^\circ \times 0.01^\circ$ grid. A grid point was considered "active" if any observation point in the area over 3×3 grids around that grid point exceeded the rainfall threshold T_R. The following definitions were applied (Dixon and Wiener, 1993):

Success: Both truth and forecast grid points active

Failure: Truth grid point active and forecast grid point inactive

False alarm: Truth grid point inactive and forecast grid point active

The performance of QPN was quantified based on the following statistics (1) the probability of detection (POD), (1) the false-alarm ratio (FAR), and (2) the critical success index (CSI). The representative formulas are as follows:

$$\mathrm{POD} = \frac{n_{\mathrm{success}}}{n_{\mathrm{success}} + n_{\mathrm{failture}}} , \tag{4}$$

$$\mathrm{FAR} = \frac{n_{\mathrm{false-alarm}}}{n_{\mathrm{success}} + n_{\mathrm{false-alarm}}} , \tag{5}$$

$$\mathrm{CSI} = \frac{n_{\mathrm{success}}}{n_{\mathrm{success}} + n_{\mathrm{failture}} + n_{\mathrm{false-alarm}}} . \tag{6}$$

In this study, the precipitation threshold T_R to elevate forecast was set at 1 mm in 1 h. Initial precipitation is difficult to forecast; therefore, the forecast skill was evaluated only during the precipitation period.

6.1 *Khanun typhoon on* 10–11 *September* 2005

Figure 4a shows MTREC vectors obtained from two consecutive radar patterns at 0254 and 0300 UTC 11 September 2005. The rotation is characteristic of typhoon, and MTREC vector fields are relatively smooth and consistent. Based on the MTREC vectors, the 1-h accumulative precipitation at 0300 UTC obtained by combining radar and rain gauge data was extrapolated using a semi-Lagrangian integral scheme, and the forecast field of 1-h lead time and simultaneous observation field of 1-h precipitation are shown in Figs. 4b and c. Comparing Fig. 4b with c, the precipitation distribution of the forecast is similar to that of observation, especially with regard to the location of rotational heavy rainfall.

An evaluation of forecast skill was performed using Eqs. (4–6). The forecast result can be seen in Fig. 4d. The evaluation threshold of 1 mm h^{-1} was set, and the percent of success (Fig. 4d, green color) over most of the precipitation area was >80%, which indicates that the locations of heavy precipitation in both forecasting and observations nearly overlapped. The corresponding POD was 0.89, the FAR was 0.16, and the CSI was 0.76.

Because it is a challenge to forecast initial precipitation, the evaluation of forecast skill was performed during precipitation. Time and results are shown in Table 1. The average POD value of 0.85 at the lead time of 1 h indicates that on average 85% of the forecasting precipitation grids overlapped with the observation precipitation. One can see from Table 1 that the average POD at a 3-h lead time is still 0.60, although the forecast skill decreased with the forecast time as expected. The predictability of precipitation increased as a function of scale (Germann and Zawadzki, 2002). The Khanun typhoon is characterized by a large area of precipitation and coherent structure, which indicates slow temporal evolution and stable shape and relatively long predictability.

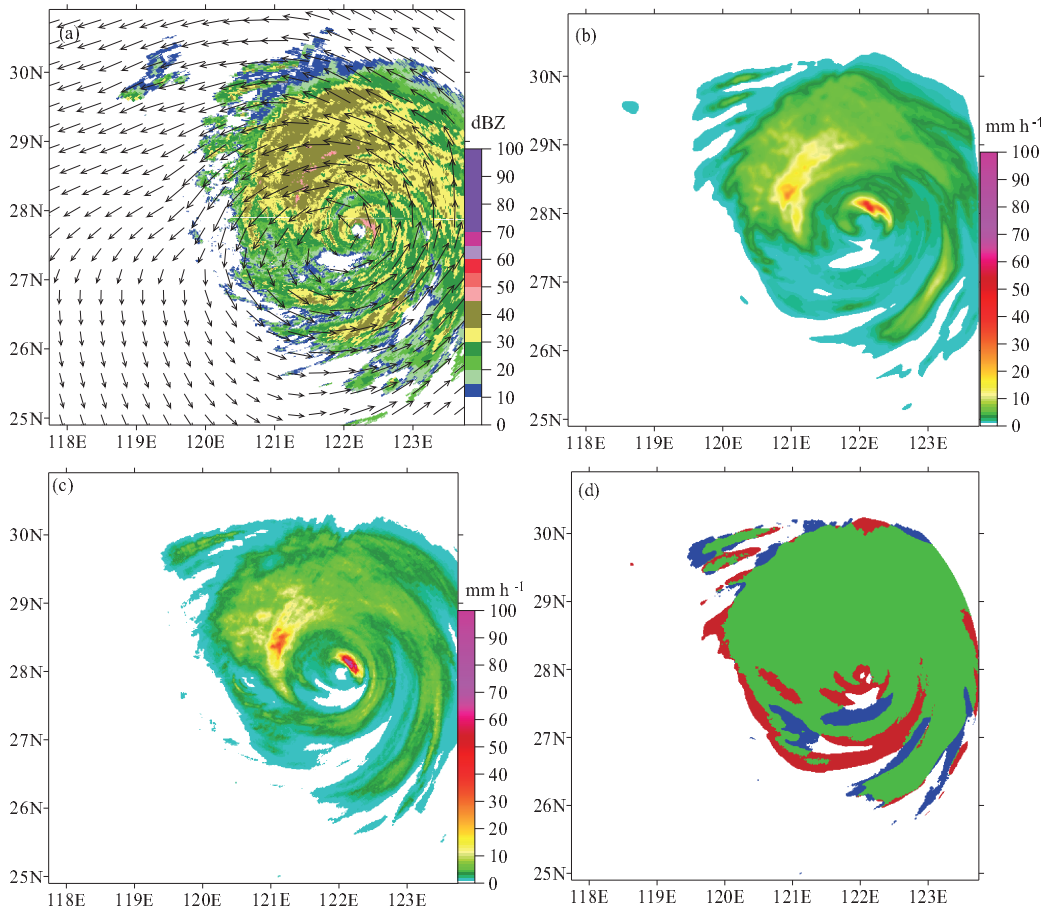

Fig. 4. (a) The MTREC vectors obtained from two consecutive radar patterns at 0254 and 0300 UTC 11 September 2005, (b) forecast precipitation at the forecast time of 1 h and (c) simultaneous observation 1 h precipitation obtained by combining radar and rain gauge, and (d) forecast evaluation, the green color expresses the area of success, the blue color expresses failure, and the red color expresses false alarm.

6.2 *Squall line on* 23 *June* 2011

Figure 5a gives the MTREC vectors obtained from two consecutive radar images at 0954 and 1000 UTC 23 June 2011. The echoes moved toward the southeast and MTREC vectors were continuous and consistent without zero vectors. Based on the MTREC vectors, the 1-h accumulative precipitation at 1000 UTC obtained by combining radar and rain gauge was extrapolated using a semi-Lagrangian advection scheme, and the 1-h lead-time forecasting result and simultaneous observation 1-h precipitation are given in Figs. 5b and c. Comparing Figs. 5b with c, the precipitation distribution of forecast was similar to that of observations, and the location of heavy rainfall mostly overlapped. Due to precipitation intensity changes over time, there were some differences in precipitation intensity; the observation precipitation was heavier than forecasting precipitation.

Table 1. Forecast evaluation for the Khanun typhoon on 11 September 2005 (evaluation threshold is 1.0 mm).

Forecast lead time	P_{OD}	F_{AR}	C_{SI}
1 h	0.85	0.19	0.72
2 h	0.71	0.29	0.59
3 h	0.60	0.41	0.48

The same procedure for the evaluation of forecast skill was repeated (Fig. 5d). The locations of heavy precipitation in both the forecast and observation data mostly overlapped. False alarms (Fig. 5d, red color) were numerous because of the limitations of the single radar observation range. The corresponding POD was 0.69, the FAR was 0.37, and the CSI was 0.49.

The evaluation of the forecast skill was repeated

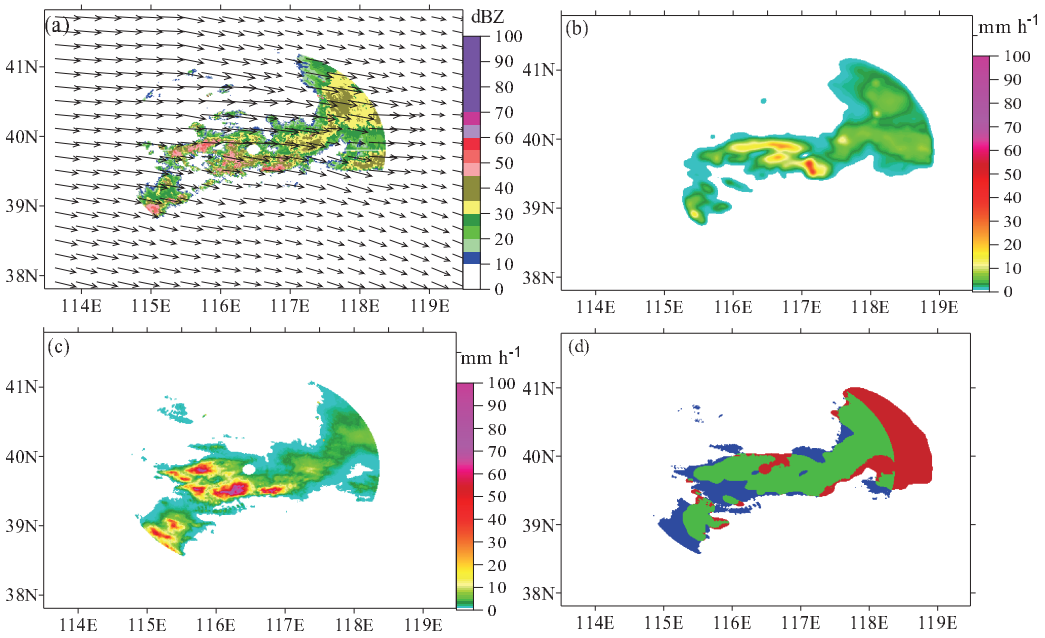

Fig. 5. (a) The MTREC vectors obtained from at 0954 and 1000 UTC 23 June 2011, (b) forecast precipitation at the forecast time of 1 h and (c) simultaneous observation 1 h precipitation obtained by combining radar and rain gauge, and (d) forecast evaluation, the green color expresses the area of success, the blue color expresses failure, and the red color expresses false alarm.

during precipitation time (Table 2). The POD value of 0.65 at lead time of 1 h indicates that, on average, 65% of the forecast precipitation area overlapped with the observation precipitation. Forecast skill decreased rapidly with forecast time. The POD value at a 3-h lead time was 0.35, which was much less than the POD value of the Khanun typhoon. In the squall-line case, 9% of the precipitation area showed rainfall rates >10 mm h^{-1}. Convective cells were predominant, which resulted in fast temporal evolution and shape change and relatively low predictability.

7. Summary

Movements of echoes at different scales are not always consistent, and zero vectors often exist in TREC and COTREC vectors. In this study, a multi-scale tracking radar echoes method based on cross-correlation (MTREC) was proposed. The MTREC scheme first determined systematic movement between two consecutive images using the TREC technique with a large "box", then the small-scale internal motions were obtained using the TREC technique with a small "box". At last, the individual motion vectors were obtained by combining the systematic movement and the individual internal motion vectors. To reduce the influence of "noisy" vectors, verification of data consistency and objective analyses were performed.

Table 2. Forecast evaluation for the squall line on 23 June 2005 (evaluation threshold is 1.0 mm).

Forecast lead time	POD	FAR	CSI
1 h	0.65	0.39	0.47
2 h	0.47	0.49	0.31
3 h	0.35	0.61	0.20

Performance of the MTREC technique was compared with the TREC technique and radar Doppler measurements using two case studies: the Khanun Typhoon (0515) on 11 September 2005 observed by Wenzhou CINRAD/SA radar and a squall line system on 23 July 2011 observed by Beijing CINRAD/SA radar. The results demonstrate that MTREC not only could track the systemic movement of the entire radar echo but also could make the individual motion vectors smoother and more continuous. One advantage of the MTREC technique is that zero vectors were eliminated where the motion field over the null echo region was specified by the large-scale motion vectors for the entire radar reflectivity pattern.

The MTREC was used for QPN, and radar data and rain-gauge measurements of the two heavy precipitation events were collected for evaluating QPN. The precipitation fields obtained by combining radar and rain gauge data were extrapolated to produce QPN fields using MTREC. The results show that MTREC

vectors are smoother and more continuous. The location of heavy precipitation at lead time of 1 h matched that of radar QPE. The accuracy of extrapolation decreased rapidly with lead time because of difficulties in treating initiation, storm evolution, and variations in storm motion (Mueller et al., 2003). On the other hand, the mesoscale numerical weather prediction model, which assimilates a variety of high-resolution observations, has been developed in recent years, and the forecast accuracy is relatively stable. Therefore, recent developments suggest that a viable way to improve the 1–6-h QPF is through the blending of extrapolation, expert system technique, and numerical weather prediction methods (Wilson and Xu, 2006; Wang et al., 2009). The globe/regional assimilation and prediction system-mesoscale model (GRAPES-meso) has been developing by the State Key Laboratory of Severe Weather of the Chinese Academy of Meteorological Science; the focus of our future research will be to blend radar echoes extrapolation and GRAPES-meso to improve the forecast skill of 1–6-h QPF.

Acknowledgements. This study was supported by the Special Fund for Basic Research and Operation of Chinese Academy of Meteorological Science: Development on quantitative precipitation forecasts for 0–6 h lead times by blending radar-based extrapolation and GRAPES-meso, Observation and retrieval methods of micro-physics parameters of atmospheric hydrometeor and wind field vertical structure with multi-wavelength remote sensing; the National Natural Science Foundation of China (Grant No. 40975014). The authors also thank DING Yuanyuan for processing much of the data and the two anonymous reviewers for their helpful comments on the original manuscript.

REFERENCES

Baeck, M., and J. Smith, 1998: Rainfall estimation by the WSR-88D for heavy rainfall events. *Wea. Forecasting*, **13**, 416–436.

Dixon, M., and G. Wiener, 1993: TITAN: Thunderstorm identification, tracking, analysis and nowcasting—A radar-based methodology. *J. Atmos. Oceanic Technol.*, **10**, 785–797.

French, M., W. Krajewski, and R. Cuykendall, 1992: Rainfall forecasting in space and time using a neural network. *J. Hydrol.*, **137**, 1–31.

Germann, U., and I. Zawadzki, 2002: Scale-dependence of the predictability of precipitation from continental radar images. Part I: Description of the methodology. *Wea. Mon. Rev.*, **130**(12), doi: 10.1175/1520-0493(2002)130.

Germann, U., I. Zawadzki, and B. Turner, 2006: Predictability of precipitation from continental radar images. Part IV: Limits to prediction. *J. Atmos. Sci.*, **63**, 2092–2018.

Han, L., S. X. Fu, L. F. Zhao, Y. G. Zhao, H. Q. Wang, and Y. J Lin, 2009: 3D convective storm identification, tracking, and forecasting—An enhanced TITAN algorithm. *J. Atmos. Oceanic Technol.*, **26**, 719–732.

Houze, R. A., W. Schmid, R. G. Fovell, and H. H. Schiesser, 1993: Hailstorms in Switzerland: Left movers, right movers, and false hooks. *Mon. Wea. Rev.*, **121**, 3345–3370.

Johnson, J., P. Mackeen, A. Witt, E. Mitchell, G. Stumpf, M. Eilts, and K. Thomas, 1998: The storm cell identification and tracking algorithm: An enhanced WSR-88D algorithm. *Wea. Forecasting*, **13**, 263–276.

Kessler, E., and J. A. Russo, 1963: Statistical properties of weather echoes. Preprints, *10th Weather Radar Conf.*, Washington, DC, Amer. Meteor. Soc., 25–33.

Lakshmanan, V., R. Rabin, and V. DeBrunner, 2000: Identifying and tracking storms insatellite images. 2*nd Artificial Intelligence Conference*, Amer. Meteor. Soc., Long Beach, CA, 90–95.

Lakshmanan, V., R. Rabin, and V. DeBrunner, 2003: Multiscale storm identification and forecast. *J. Atmos. Res.*, **4**, 367–380.

Li, L., W. Schmid, and J. Joss, 1995: Nowcasting of motion and growth of precipitation with radar over a complex orography. *J. Appl. Meteor.*, **34**, 1286–1300.

Li, P. W., W. K.Wong, K. Y. Chan, and S. T. Lai, 2000: SWIRLS—An evolving nowcasting system. Technical Note No. 100, 33pp.

Li, Y. D., J. W. Liu, and S. T. Gao, 2004: On the progress of application for dynamic and energetic convective parameters associated with severe convective weather forecasting. *Acta Meteorologica Sinica*, **62**(4), 401–408. (in Chinese)

Liang, Q. Q., Y. R. Feng, W. J. Deng, S. Hu, Y. Y. Huang, Q. Zeng, and Z. T. Chen, 2010: A composite approach of radar echo extrapolation based on TREC vectors in combination with model-predicted winds. *Adv. Atmos. Sci.*, **27**(5), 1119–1130, doi: 10.1007/s00376-009-9093-4.

Mueller, C., T. Saxen, R. Roberts, J. Wilson, T. Betancourt, S. Dettling, N. Oien, and J. Lee, 2003: NCAR auto-nowcast system. *Wea. Forecasting*, **18**, 545–561.

Pradeep, V. M., U. Germann, L. Panziera, and A. Hering, 2012: Can Lagrangian extrapolation of radar fields be used for precipitation nowcasting over complex Alpine orography? *Wea. Forecasting*, doi: 10.1175/WAF-D-11-00050.1.

Pierce, E., and Coauthors, 2004: The nowcasting of precipitation during Sydney 2000: An appraisal of the QPF algorithms. *Wea. Forecasting*, **19**, 7–21.

Reich, S., 2007: An explicit and conservative remapping strategy for semi-Lagrangian advection. *Atmos. Sci. Lett.*, **8**, 58–63.

Rinehart, R. E., 1981: A pattern recognition technique for use with conventional weather radar to determine internal storm motions. *J. Atmos. Oceanic Technol.*,

13, 119–134.

Rinehart, R. E., and E. Garvey, 1978: Three-dimensional storm motion detection by conventional weather radar. *Nature*, **273**, 287–289.

Steiner, M., R. A. Houze, and S. E. Yuter, 1995: Climatological characterization of three-dimensional storm structure from operational radar and rain gauge data. *J. Appl. Meteor.*, **34**, 1978–2007.

Tuttle, J. D., and G. B. Foote, 1990: Determination of the boundary layer airflow from a single doppler radar. *J. Atmos. Oceanic Technol.,* **7**, 218–232.

Tuttle, J., and R. Gall, 1999: A single-radar technique for estimating the winds in tropical cyclones. *Bull. Amer. Meteor. Soc.*, **80**, 653–668.

Wang, G. L., L. P. LIU, and Y. Y. Ding, 2012: Improvement of radar quantitative precipitation estimation based on real-time adjustments to Z–R relationships and inverse distance weighting correction schemes. *Adv. Atmos. Sci.*, **29**(2), 575–584, doi: 10.1007/s00376-011-1139-8.

Wang, G. L., L. P. Liu, and Z. Ruan, 2007: Application of Doppler radar data to nowcasting of heavy rainfall. *Journal of Applied Meteorological Science.* **18**(2), 388–395. (in Chinese)

Wang, H. Y., L. P. Liu, G. L. Wang, W. Zhang, Z. Q. Zhang, and X. L. Chen, 2009: Development and application of the Doppler weather radar 3-D digital mosaic system. *Journal of Applied Meteorological Science*, **20**(2), 241–224. (in Chinese)

Ware, E. C., 2005: Corrections to radar-estimated precipitation using observed rain gaugedata. M.S. thesis, Cornell University, 87pp.

Wilson, J. W., and E. A. Brandes, 1979: Radar measurement of rainfall—A summary. *Bull. Amer. Meteor. Soc.*, **60**(9), 1048–1058.

Wilson, J., and M. Xu, 2006: Experiments in blending radar echo extrapolation and NWP for nowcasting convective storms. *Proc. 4th European Conference on Radar in Meteorology and Hydrology*, Barcelona, Spain, 519–522

Wolfson, M., B. Forman, R. Hallowell, and M. Moore, 1999: The growth and decay storm tracker. Preprints, 8*th Conference on Aviation*, Dallas, TX, Amer. Meteor. Soc., 58–62.

Xiao, Y. J., L. P. Liu, and Y. Shi, 2008: Study of methods for three-dimensional multiple-radar reflectivity mosaics. *Acta Meteorologica Sinica*, **22**(2), 370 –380.

Yao, J. H., J. H. Dai, and Z. Q. Yao, 2005: Case analysis of the formation and evolution of 12 July 2004 severe squall line. *Journal of Applied Meteorological Science*, **16**(6), 746–754. (in Chinese)

Zawadzki, I., 1984: Factors affecting the precision of radar measurements of rain. Preprints, 22*nd Int. Conf. on Radar Meteorology*, Zurich, Switzerland, Amer. Meteor. Soc., 251–256.

Zhang, P. C., B. Y. Du, and T. P. Dai, 2001: *Radar Meteorology.* China Meteorological Press, 511pp. (in Chinese)

Zhang, Y. P., M. H. Chen, W. M. Xia, Z. H. Cui, and H. P. Yang, 2006: Estimation of weather radar echo motion field and its application to precipitation nowcasting. *Acta Meteorologica Sinica*, **64**(5), 631–646. (in Chinese)